


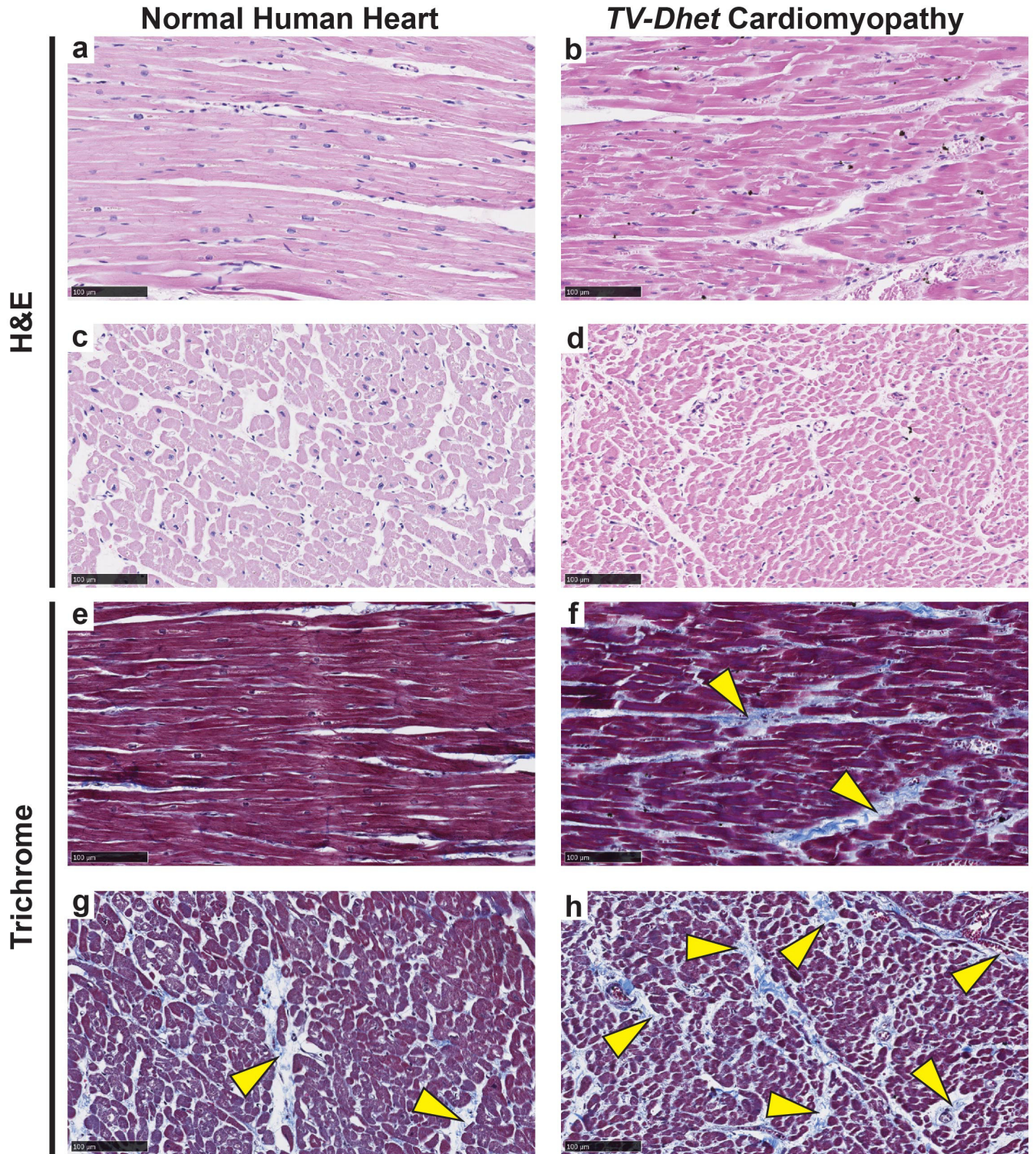


In the format provided by the authors and unedited.

Combinatorial interactions of genetic variants in human cardiomyopathy

Dekker C. Deacon^{1,8}, Cassandra L. Happe^{2,8}, Chao Chen^{1,8}, Neil Tedeschi¹, Ana Maria Manso^{1,3}, Ting Li¹, Nancy D. Dalton¹, Qian Peng ^{4,5}, Elie N. Farah¹, Yusu Gu¹, Kevin P. Tenerelli², Vivien D. Tran², Ju Chen¹, Kirk L. Peterson¹, Nicholas J. Schork⁵, Eric D. Adler¹, Adam J. Engler ^{2,6*}, Robert S. Ross ^{1,3*} and Neil C. Chi ^{1,7*}

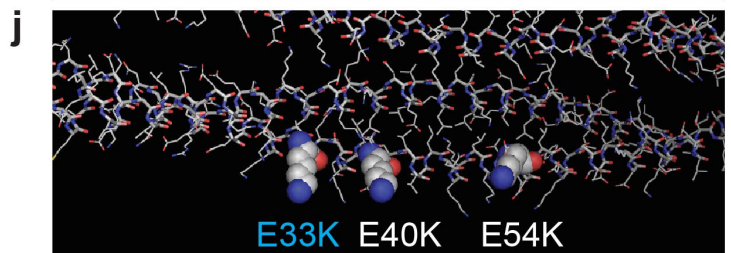
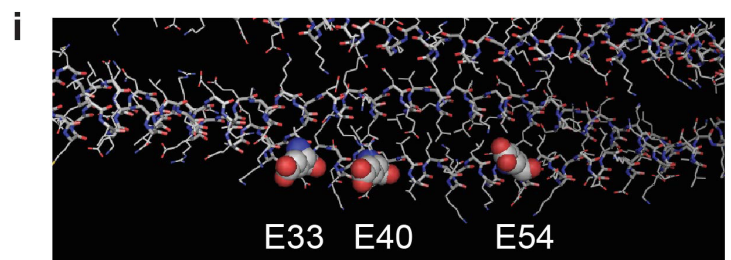
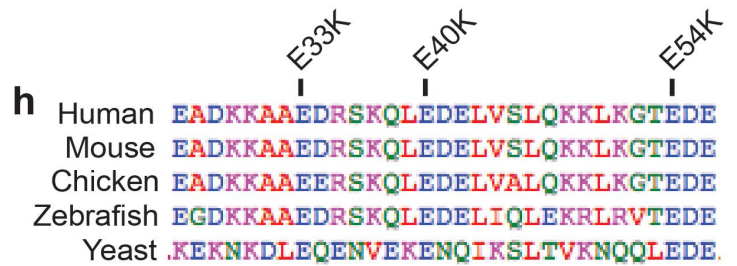
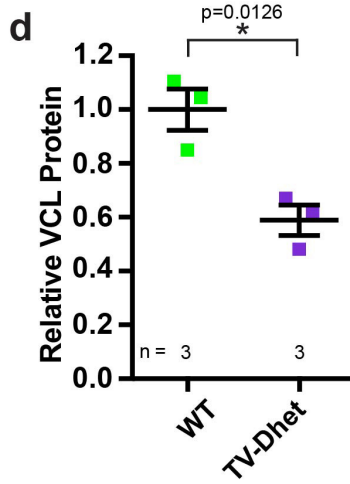
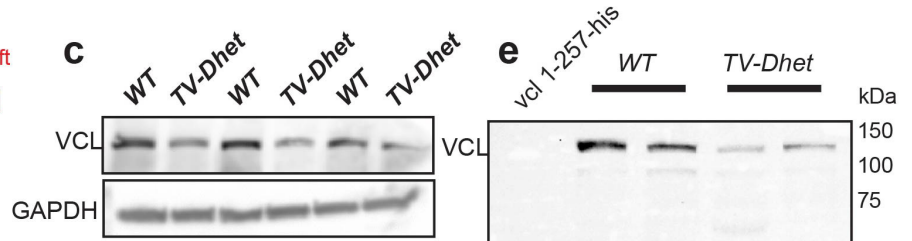
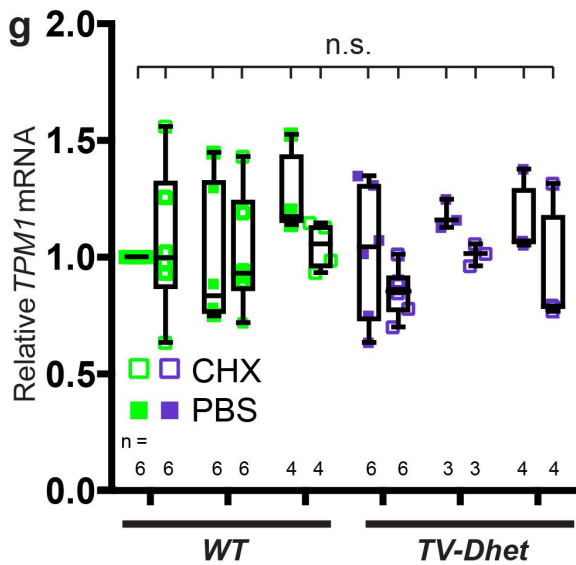
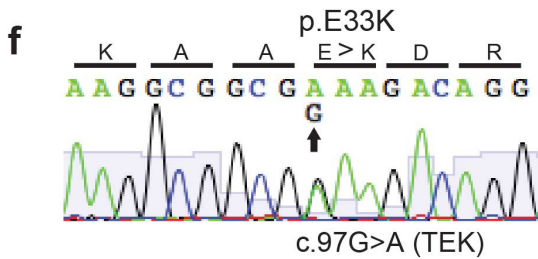
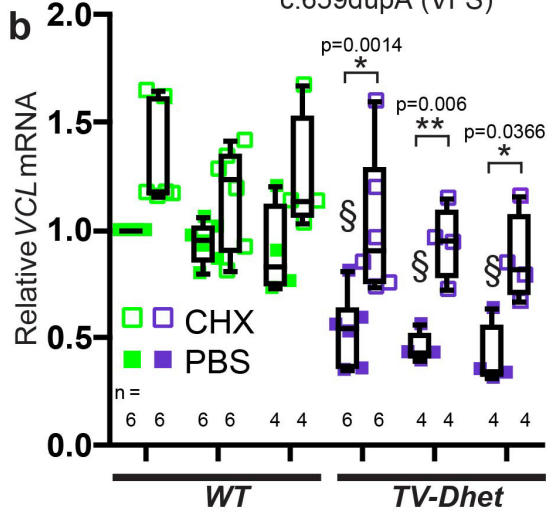
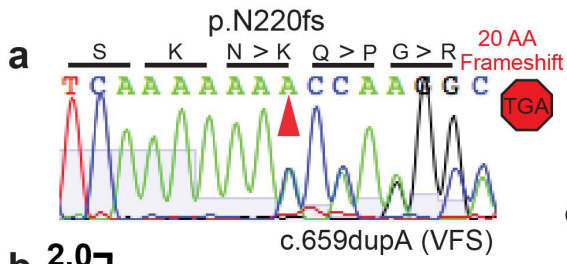
¹Division of Cardiology, Department of Medicine, University of California, San Diego, La Jolla, CA, USA. ²Department of Bioengineering, University of California, San Diego, La Jolla, CA, USA. ³Veterans Administration Healthcare San Diego, San Diego, CA, USA. ⁴Department of Neuroscience, The Scripps Research Institute, La Jolla, CA, USA. ⁵Department of Human Biology, J. Craig Venter Institute, La Jolla, CA, USA. ⁶Sanford Consortium for Regenerative Medicine, La Jolla, CA, USA. ⁷Institute of Genomic Medicine, University of California, San Diego, La Jolla, CA, USA. ⁸These authors contributed equally: Dekker C. Deacon, Cassandra L. Happe, Chao Chen. *e-mail: aengler@ucsd.edu; rross@ucsd.edu; nchi@ucsd.edu



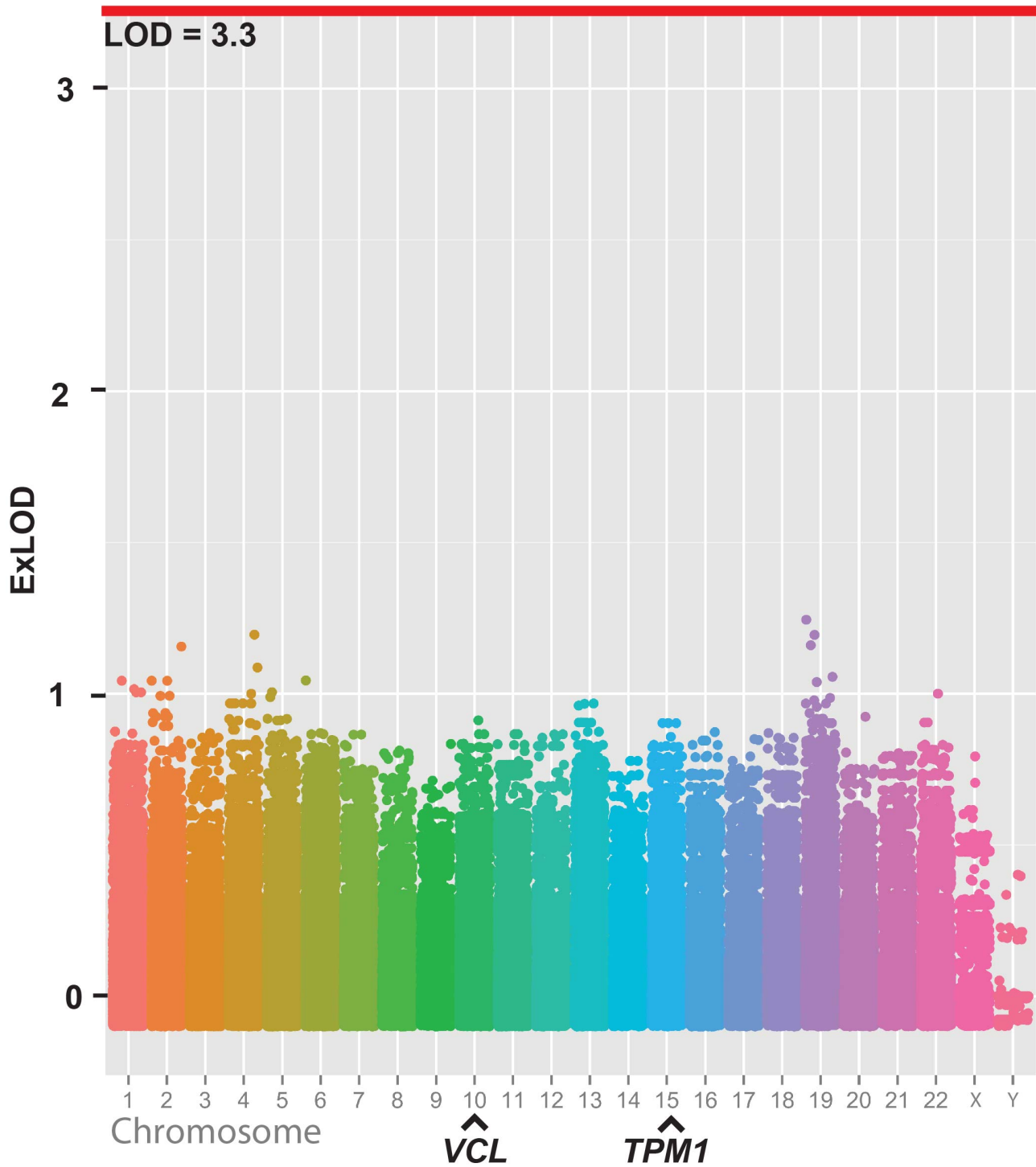
Supplementary Figure 1. Cardiac fibrosis is increased in the left ventricle of a *TV-Dhet* cardiomyopathy patient (Patient C, Fig. 1). Compared to normal human hearts (**a, c, e, g**), Patient C's cardiac tissue exhibits increased fibrosis (**b, d, f, h**). Yellow arrowheads point to interstitial and perivascular fibrosis. H&E – haematoxylin and eosin. Scale bars – 100 μ M. The data shown in panels **a-h** are representative sections from individual patients. These experiments were repeated using three separate left ventricular samples independently processed and imaged with similar results.

Supplementary Figure 2

Deacon et al.

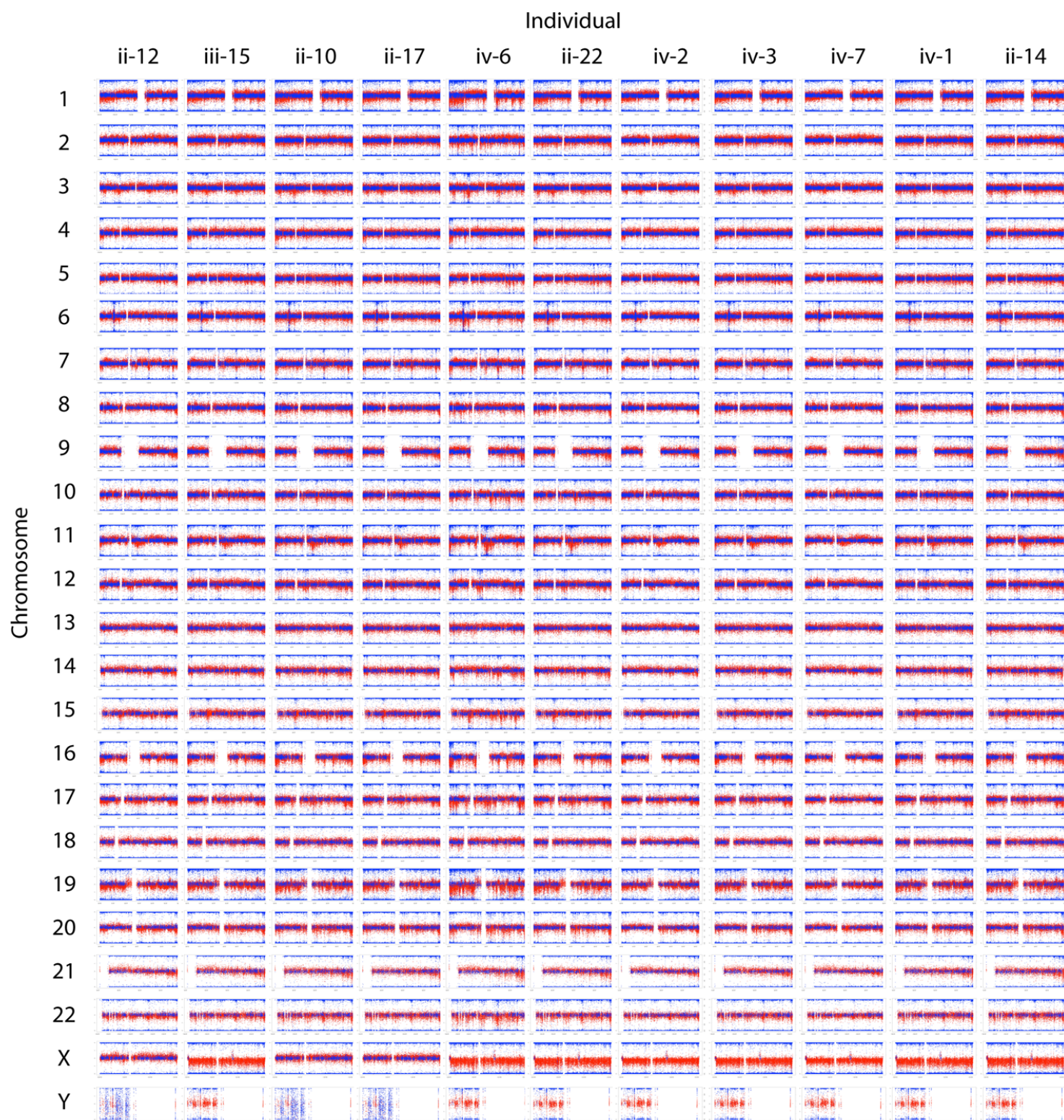


Supplementary Figure 2. Novel *VCL* and *TPM1* variants lead to decreased VCL protein expression and alteration of conserved TPM1 surface charge. (a) The *VCL* c.659dupA (*VFS*) variant (red arrowhead) leads to a shift in the reading frame of *VCL* (p.N220fs) and a premature stop 20 codons downstream. (b) qRT-PCR shows that *VCL* mRNA levels are decreased in three independent *TV-Dhet* fibroblast lines compared to *WT* controls at baseline [vehicle (PBS) treated – filled squares]. Adding cycloheximide (CHX, hollow squares) restores *VCL* mRNA levels to near-*WT* levels in *TV-Dhet* fibroblasts (* indicates $p < 0.05$ in CHX vs PBS treated cells using two-sided Student's *t*-test, $n =$ biological replicates per each of three independent fibroblast lines per genotype). § indicates $p < 0.0001$ compared to average of PBS-treated *WT* (from left to right, §: $p = 2.22e-6$, $p = 3.49e-6$, $p = 3.81e-7$) using two-sided Student's *t*-test. (c-e) Western blot analysis reveals that (c, d) VCL protein levels are decreased in *TV-Dhet* fibroblasts compared to *WT* (GAPDH loading control) (data presented as mean \pm SEM, with superimposed individual data points, $n = 3$ biological replicates per genotype, two-sided Student's *t*-test) and (e) *TV-Dhet* fibroblasts do not express an N-terminal truncated product. An N-terminal specific anti-*VCL* antibody, which recognizes a *g.gallus* vcl 1-257 peptide is unable to detect a potential VCL truncated protein (26.8kDa) in *TV-Dhet* fibroblasts. (f) The *TPM1* c.97G>A (*TEK*) variant (black arrow) results in an amino acid change from a negatively charged glutamic acid to a positively charged lysine residue at position 33 (p.E33K). (g) *TPM1* mRNA levels are not significantly (n.s.) different between *WT* and *TV-Dhet* fibroblasts at baseline (PBS; filled squares) or when treated with CHX (hollow squares) ($n =$ biological replicates per each of three independent fibroblast lines per genotype, using two-sided Student's *t*-test). (h) TPM1 E33, E40, and E54 are highly conserved amino acid residues. (i, j) Schematic of the N-terminal region of human TPM1 protein generated using PyMOL¹. The TPM1 E33K variation substitutes a negatively charged (red) glutamate residue with a positively charged (blue) lysine on the surface of the TPM1 molecule adjacent to previously reported, DCM-associated substitutions in TPM1 (E40K and E54K)². qRT-PCR data presented as interquartile range (box), surrounding data mean at center line with whiskers representing minimum and maximum of data set, with superimposed individual data points.

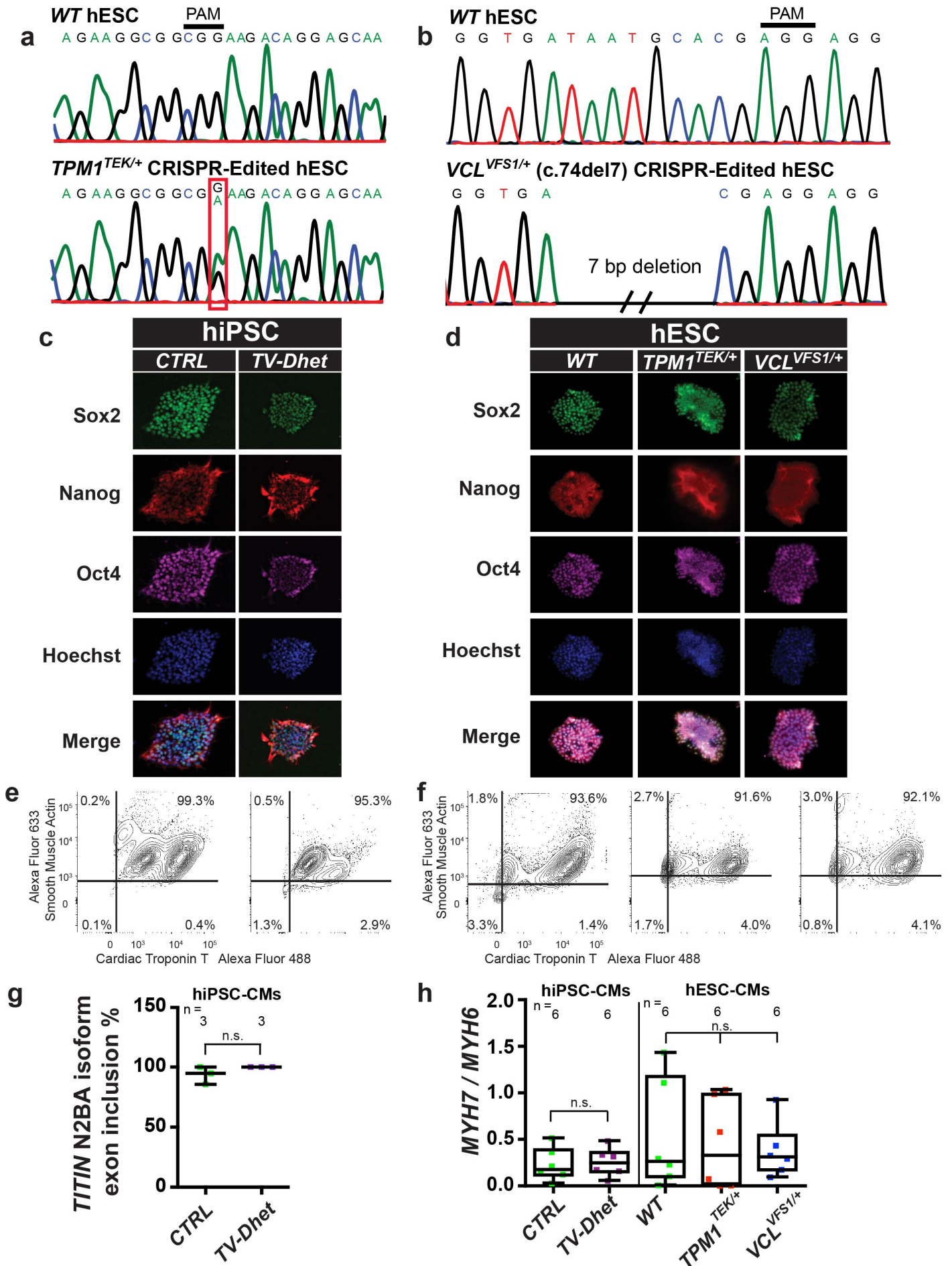


Supplementary Figure 3. No single chromosomal segment segregates with disease in DCM family. Non-parametric LOD scores (ExLOD)(Y-axis), which are calculated using the Kong and Cox³ one-sided, non-parametric linkage analysis linear model, from individuals marked with a black “Linkage Analysis” dot in **Fig. 1** (n = 11 individuals), show no chromosomal segments that are significantly associated with disease. Potential single variants maximally cosegregating with disease within this cohort (Theta = 0) would yield a significant ExLOD score of 3.3 (red line). Power to detect significant linkage disequilibrium with $p < 0.05$ was calculated to be 80% using the Genetic Power Calculator module for case-control for discrete traits (a two-sided test)⁴. Chromosomal regions of *TPMI* and *VCL* do not independently cosegregate with disease.

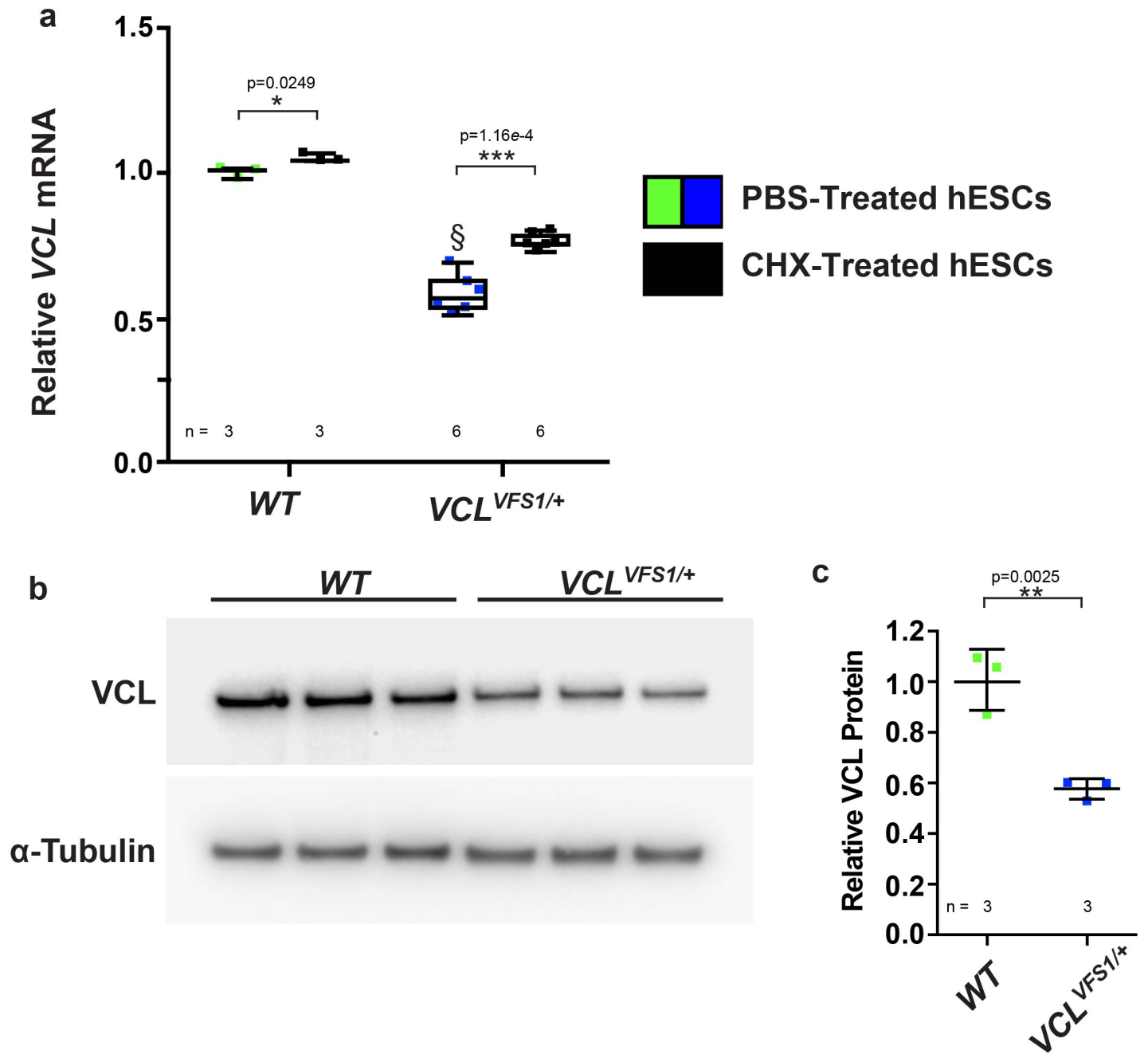
Supplementary Figure 4



Supplementary Figure 4. No large structural variation is present in chromosomes from family members diagnosed with cardiomyopathy. Log R Ratio (LRR, red), and B Allele Frequency (BAF, blue), are represented along each chromosome, for each individual analyzed with SNV-array chips. Loss of heterozygosity due to large duplications or deletions would be manifested as a shift from the midline for either parameter. However, no significant shift from the midline is evident in any chromosome (with the exception of the sex chromosomes, which vary because of the individuals' gender) including the chromosomes of cardiomyopathy-affected individuals: ii-12, iii-15, iv-2, and iv-7. Individuals are represented by their position in the pedigree as denoted by Roman numerals for the generation, and individual number for specific individual within that generation (from left to right).

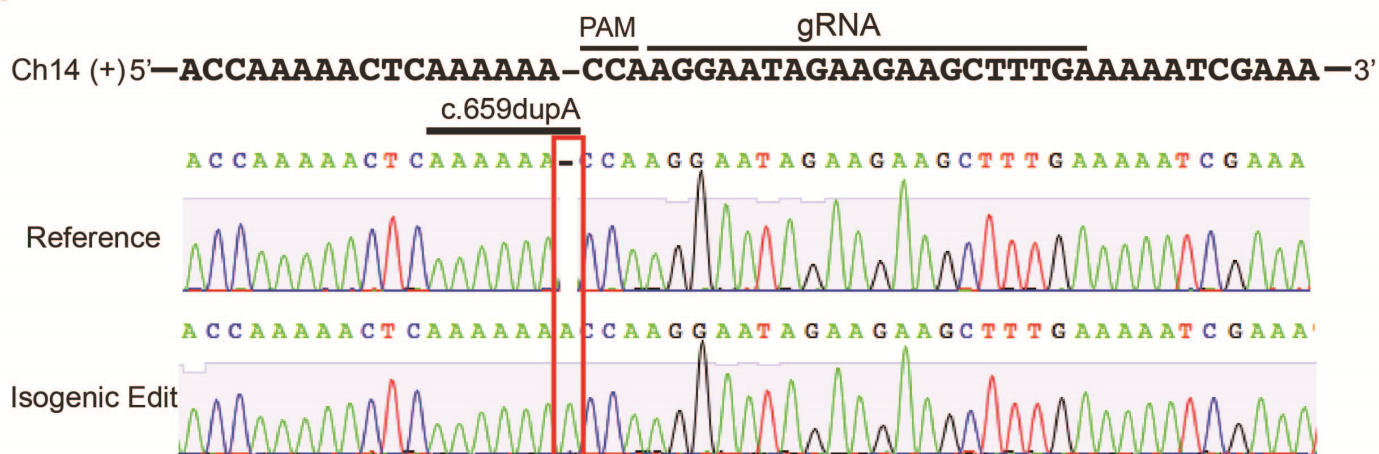


Supplementary Figure 5. Generation and differentiation of CRISPR-edited human embryonic stem cell (hESC) and patient-derived human induced pluripotent stem cell (hiPSC) lines. (a, b) Sanger sequencing confirms that CRISPR genome-edited *TEK* and *VCL* frame shift (*VFSI*) hESC lines contain (a) the *TPMI* c.G97A (*TEK*) mutation (red box), and (b) a 7 base pair deletion in *VCL* (*VCL* c.74del7 - *VFSI*), respectively. PAM - Protospacer adjacent motif. hiPSC lines (c) derived from unaffected family member (control, *CTRL*) and *TV-Dhet* patient fibroblasts, as well as genome-edited hESC lines (d) containing the *TEK* variant ($TPM^{TEK/+}$), the *VFSI* variant ($VCL^{VFSI/+}$) or no introduced variants (control, *WT*), express the pluripotency markers SOX2, NANOG, and POU5F1 (OCT4). Flow cytometry with Smooth Muscle Actin and Cardiac Troponin T reveals that (e) hiPSC and (f) hESC lines efficiently differentiate to cardiomyocytes using a cardiac differentiation monolayer protocol⁵ ($n > 10,000$ cells per genotype). Data from panels a-f were independently repeated 3 times with similar results. (g) *TITIN* N2BA isoform inclusion ratio (mean +/- SEM with superimposed individual data points, $n = 3$ biologic replicates per genotype) and (h) *MYH7/MYH6* ratios (interquartile range (box), surrounding data mean at center line with whiskers representing minimum and maximum of data set, with superimposed individual data points, $n = 6$ biologic replicates per genotype) are not significantly different between compared groups [$p > 0.05$ across all comparisons, (n.s.), two-sided Student's *t*-test for panel (g) and *CTRL* vs *TV-Dhet* in panel (h), one-sided ANOVA with multiple comparison correction for *WT* vs $TPM^{TEK/+}$ vs $VCL^{VFSI/+}$ in (h)].

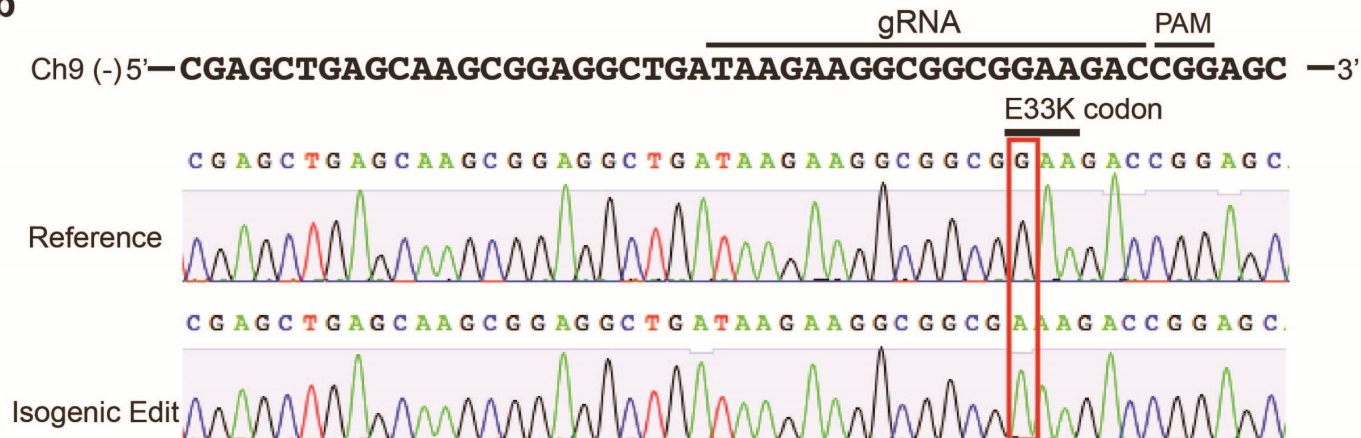


Supplementary Figure 6. *VFSI* (*VCL c.74del7*) H9 hESCs express VCL at approximately half of normal levels compared to wild type (*WT*) H9 hESCs due to nonsense-mediated mRNA decay (NMD). (a) *VCL*^{*VFSI/+*} hESCs (blue) express *VCL* mRNA at rates approximately half of control *WT* (green) hESCs when treated with vehicle (PBS). However, addition of cycloheximide (black bars) results in significantly increased *VCL* mRNA levels in *VCL*^{*VFSI/+*} hESCs. *VCL*^{*VFSI/+*} hESCs express reduced levels of VCL protein by (b) Western analysis (using α -tubulin as a loading control) and (c) densitometry analysis, which are comparable to levels observed in human and mouse cells harboring the *VCL c.659dupA* (*VFS*) variant. Data presented as mean +/- SEM or as interquartile range (box), surrounding data mean at center line with whiskers representing minimum and maximum of data set, with superimposed individual data points. Two-sided Student's *t*-test: **p* < 0.05, ***p* < 0.01, ****p* < 0.001 in CHX vs PBS treated cells. § indicates *p*=1.9e-5 for *WT* vs *VFSI* PBS treated cells (n = 6 biological replicates for *VCL*^{*VFSI/+*} hESC *VCL* mRNA analysis, and n = 3 biological replicates for *WT* hESC *VCL* mRNA analysis, WT and *VCL*^{*VFSI/+*} hESC VCL protein analysis.)

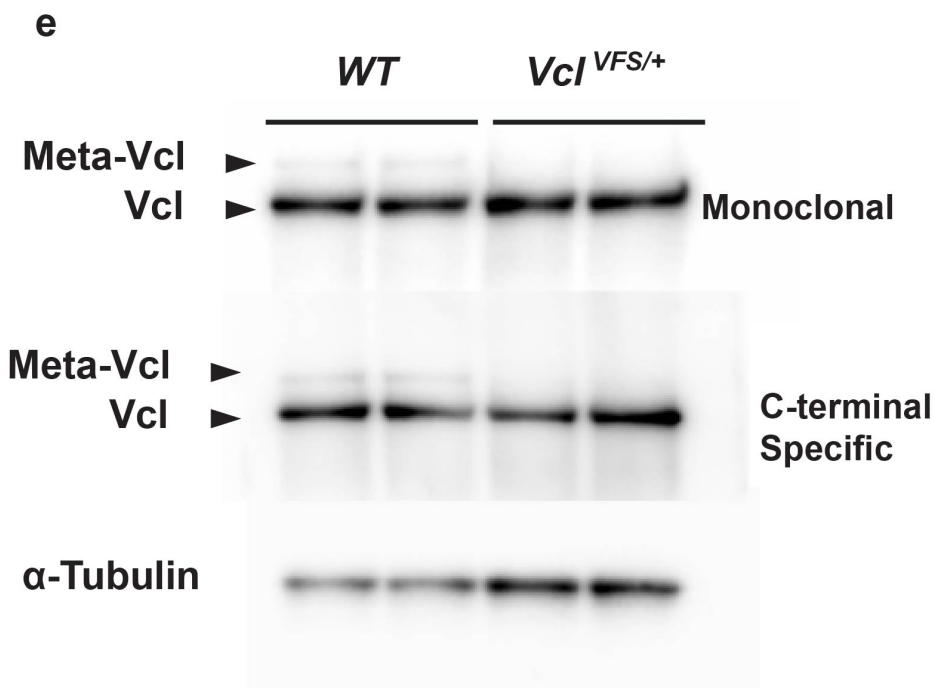
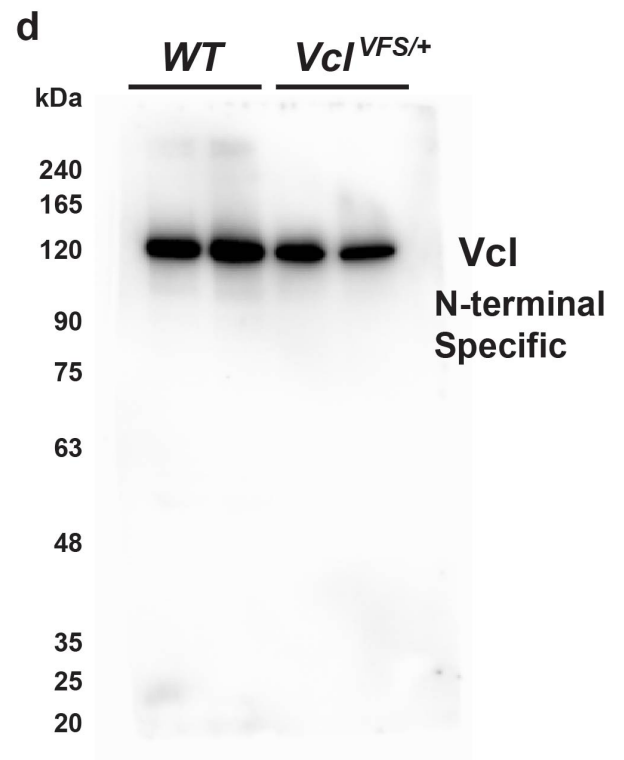
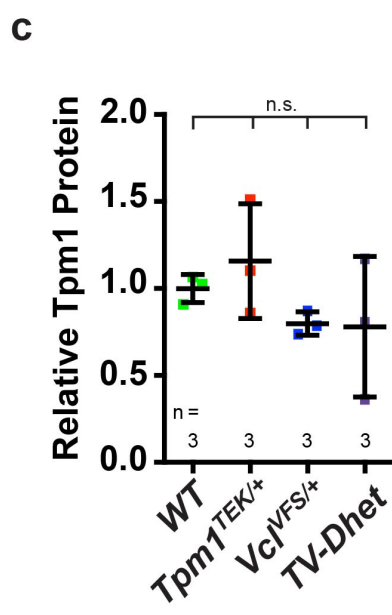
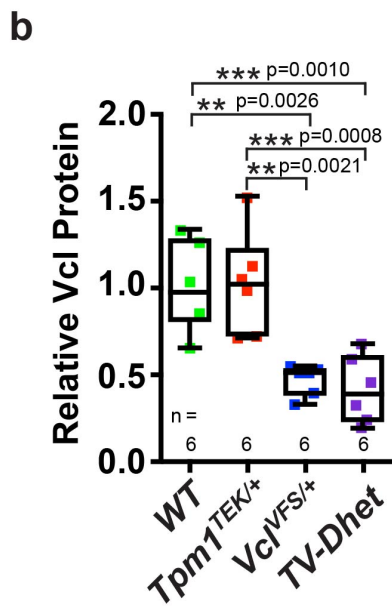
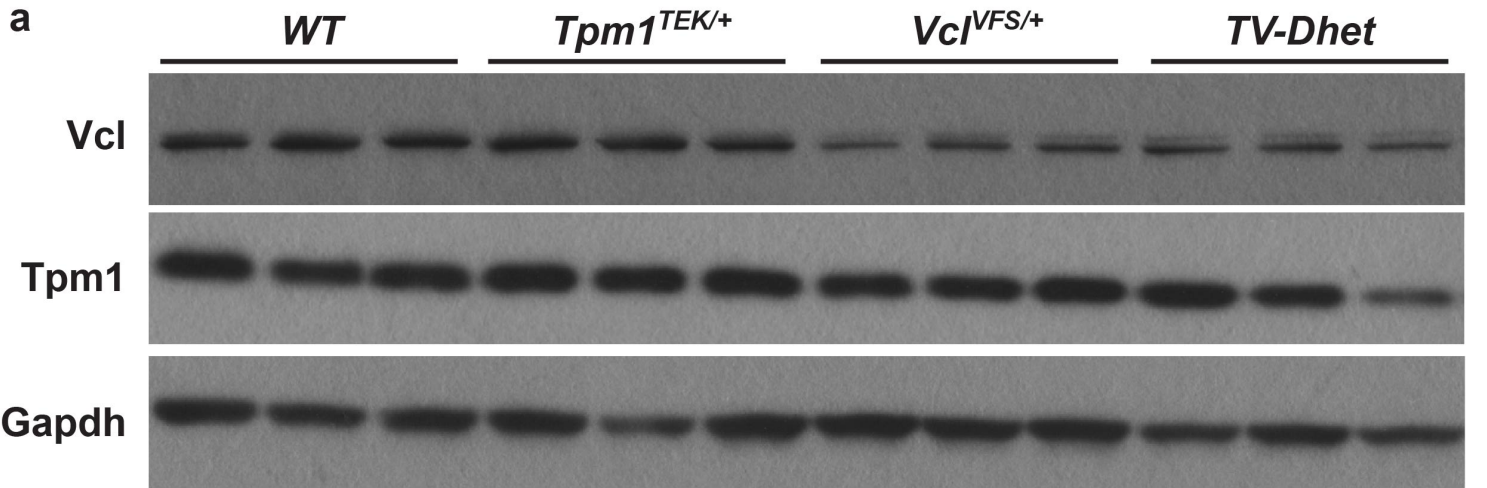
a



b



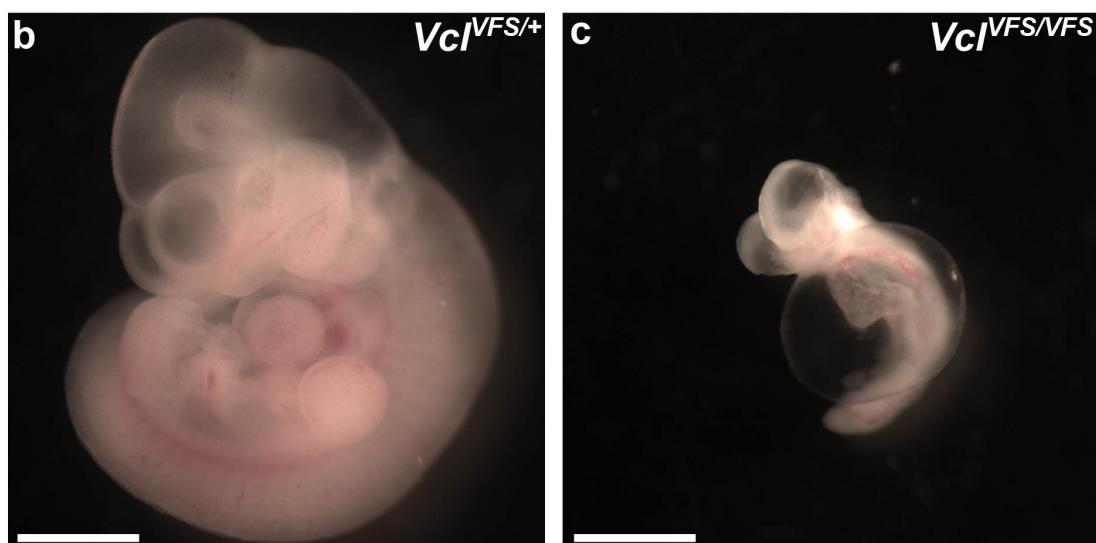
Supplementary Figure 7. DNA sequencing confirms mouse CRISPR genome-edited *Vcl* c.659dupA (p.N220fs) (*VFS*) and *Tpm1* c.97G>A (p.E33K) (*TEK*) variants. Sanger sequencing from PCR clones of gDNA shows that genome-edited mice contain the patient-specific (a) *Vcl* c.659dupA (red box) and (b) *Tpm1* c.97G>A, p.E33K (red box) variants. gRNA and PAM indicate guide RNA targeting sequences and protospacer adjacent motifs used in targeting strategy. These experiments were independently repeated more than 100 times with similar results.



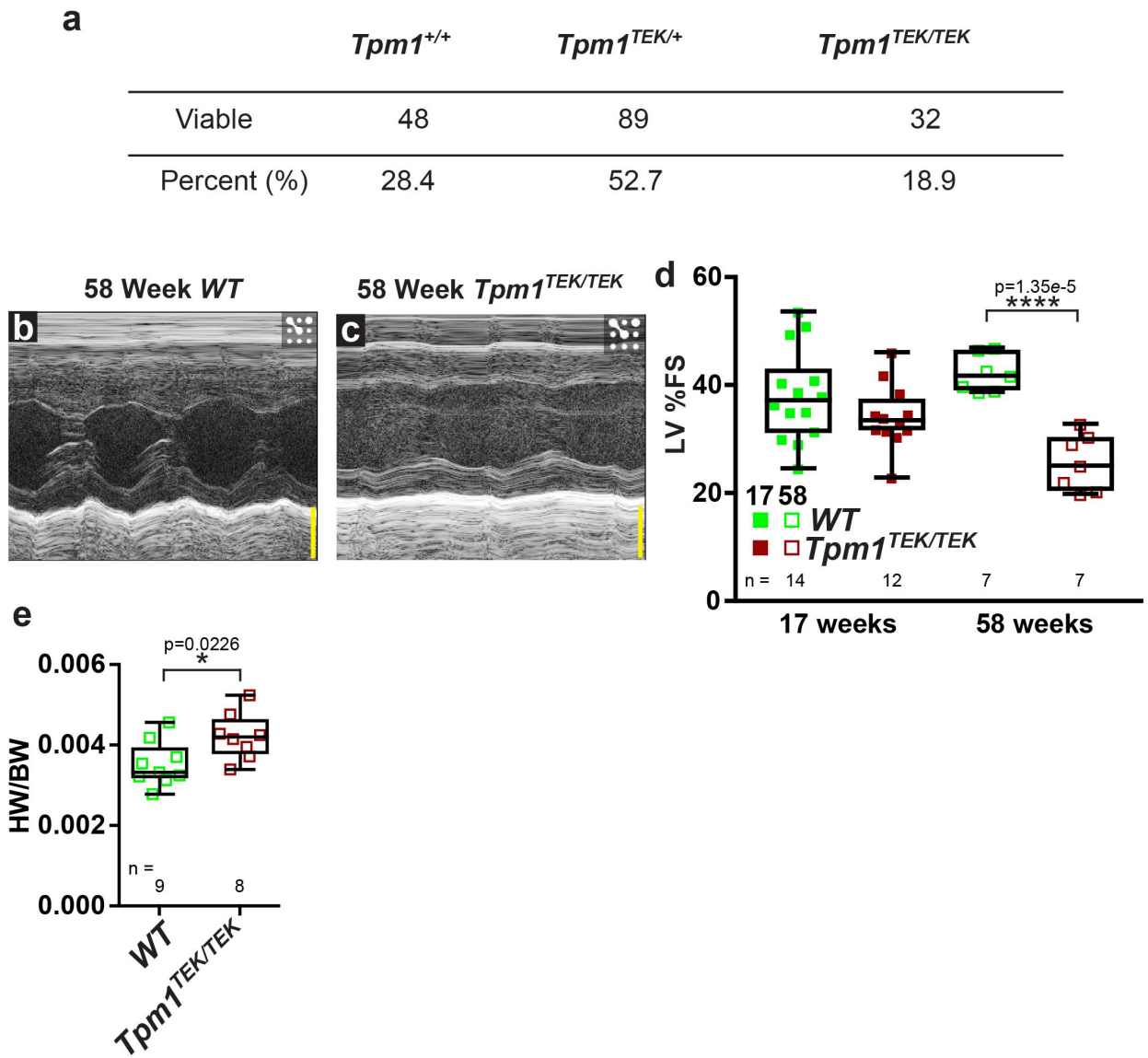
Supplementary Figure 8. Cardiac Vcl levels are reduced in $Vcl^{VFS/+}$ and *TV-Dhet* mice but cardiac Tpm1 levels are unaffected in $Tpm1^{TEK/+}$ and *TV-Dhet* mice. (a) Western blot and (b, c) densitometry analyses reveal that (b) Vcl levels in $Vcl^{VFS/+}$ and *TV-Dhet* mouse hearts are reduced compared to *WT* and $Tpm1^{TEK/+}$ mice; however, (c) Tpm1 levels are similar across all examined genotypes. Data are normalized to Gapdh levels, and presented as mean +/- SEM relative to average *WT* protein expression level, with superimposed individual data points. One-sided ANOVA with Tukey multiple correction test alpha **p < 0.01, ***p < 0.001, “n.s.” indicates no statistically significant comparisons, (n = number of independent biological replicates per genotype). (d) An anti-N-terminal Vcl antibody was unable to detect a truncated Vcl protein in either *WT* or $Vcl^{VFS/+}$ mouse hearts. (e) Full length Vcl represents the dominant translation product of the *Vcl* gene in both *WT* and $Vcl^{VFS/+}$ mice. α -tubulin was used as a loading control in d and e.

a

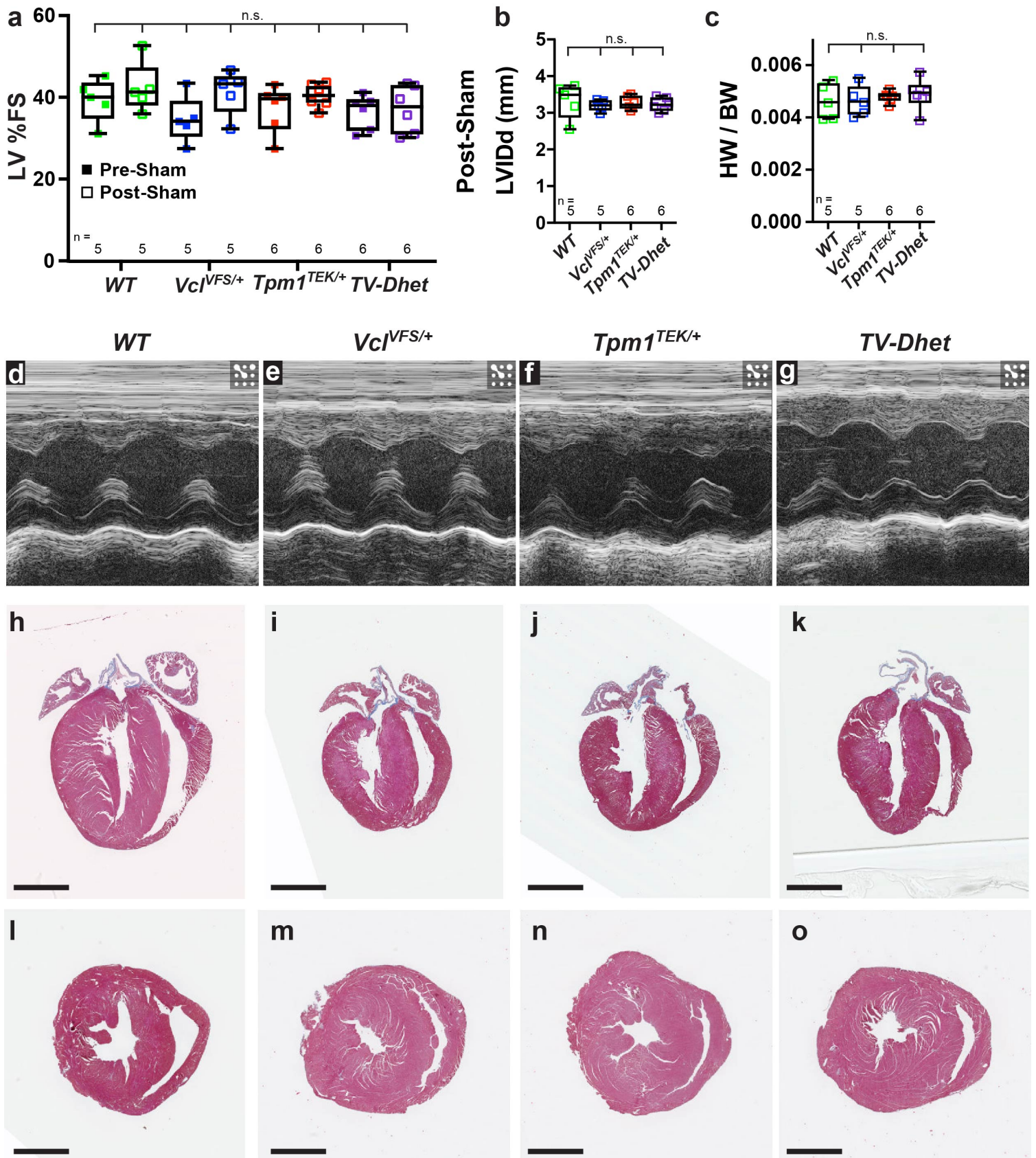
Day of Gestation	<i>Vcl</i> ^{+/+}	<i>Vcl</i> ^{VFS/+}	<i>Vcl</i> ^{VFS/VFS}	Resorbed
E9.5	5	11	4	0
E10.5	4	11	5	0
E11.5	3	2	3	0
E12.5	3	4	0	3
E13.5	4	4	0	3
Percent (%)	24.6	45.9	19.7	9.8
Viable	6	17	0	N/A



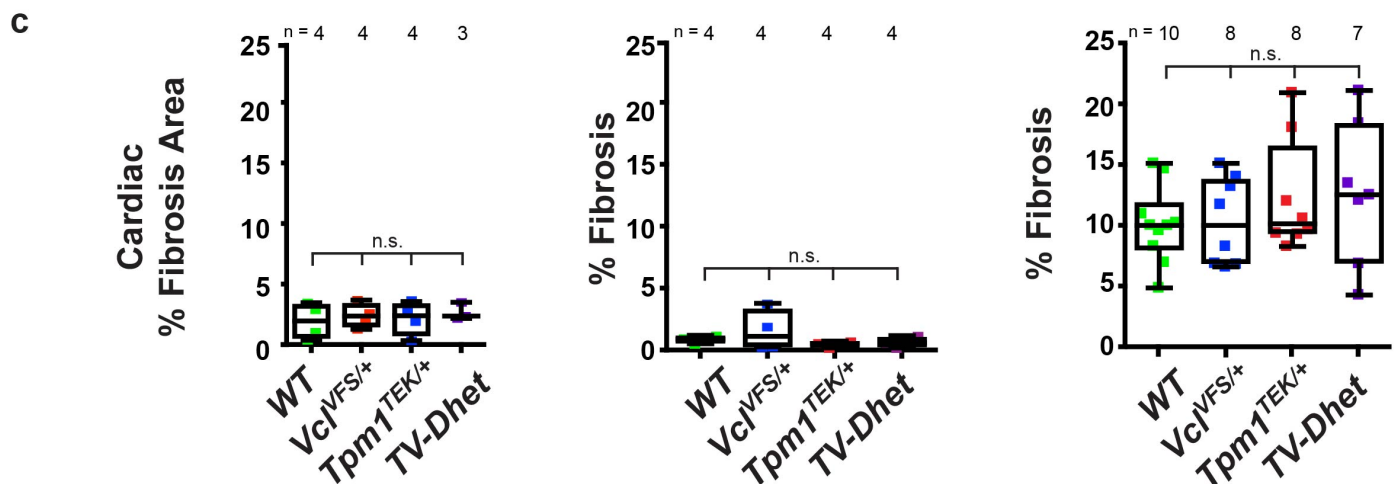
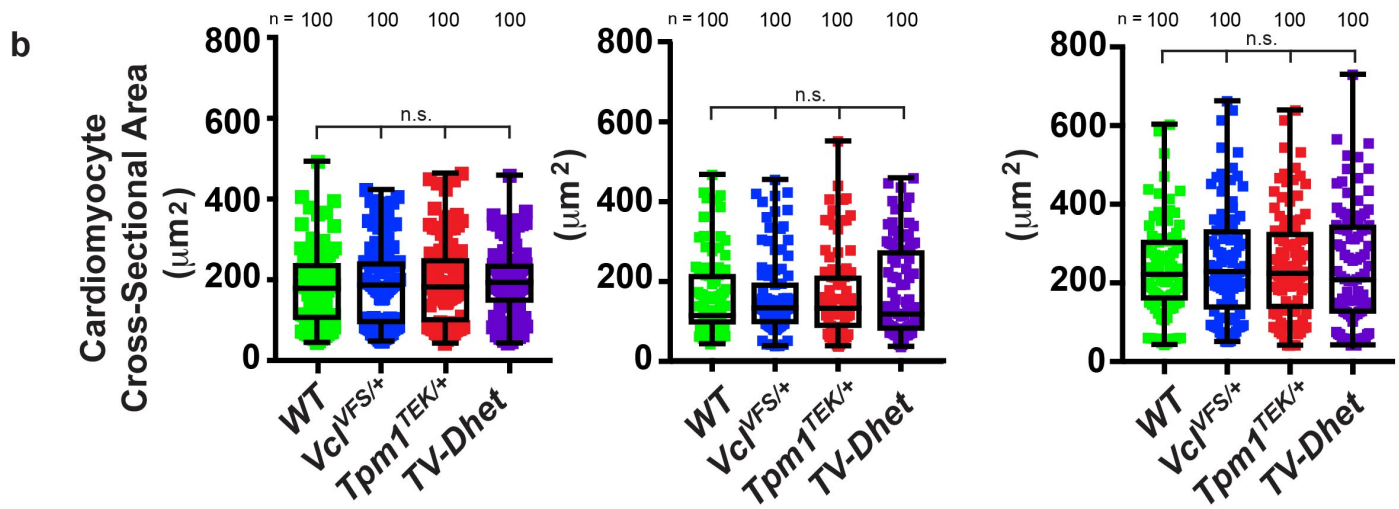
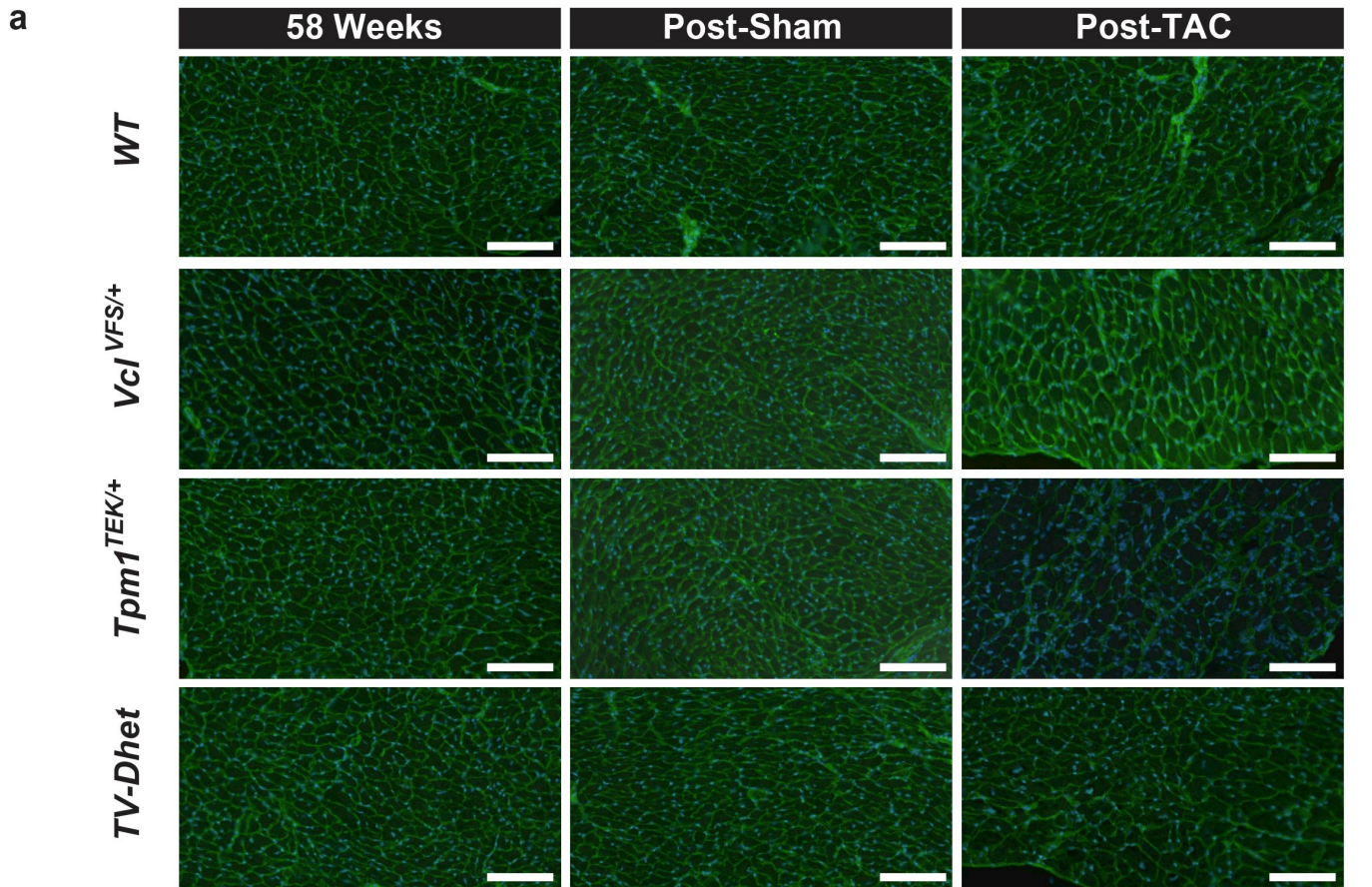
Supplementary Figure 9. The homozygous *VFS* (*Vcl* c.659dupA) variant results in a strong loss-of-function mouse allele. (a) Breeding $Vcl^{VFS/+}$ mice reveals that $Vcl^{VFS/VFS}$ animals are embryonic lethal by E12.5. **(b)** $Vcl^{VFS/+}$ mouse embryos develop normally at E10.5 but $Vcl^{VFS/VFS}$ embryos exhibit **(c)** gross abnormalities including pericardial edema and neural tube fusion defects. This experiment was independently repeated 7 times with similar results. 1 mm scale bars.



Supplementary Figure 10. *Tpm1*^{TEK/TEK} mice display decreased cardiac contractility. (a) *Tpm1*^{TEK/+} and *Tpm1*^{TEK/TEK} mice are viable and present in expected Mendelian ratios. (b-d) At 58 weeks, M-mode echocardiography reveals that left ventricular % fractional shortening (LV %FS) is significantly reduced in (c) *Tpm1*^{TEK/TEK} mouse hearts when compared to (b) *WT* mouse hearts. n = 7-14 animals per condition [17 weeks: *WT* (n = 14), *Tpm1*^{TEK/TEK} (n = 12), 58 weeks: *WT* (n = 7), *Tpm1*^{TEK/TEK} (n = 7)]. (e) Heart weight/body weight (HW/BW) ratios are significantly increased in *Tpm1*^{TEK/TEK} mice compared to *WT* at 58 weeks (n = 9 *WT* mice and 8 *Tpm1*^{TEK/TEK} mice). 2 mm scale bars. Data presented as mean +/- SEM. Two-sided Student's *t*-test: *p < 0.05, **p < 0.01, ***p < 0.001, ****p < 0.0001.



Supplementary Figure 11. Mice harboring various combinations of TEK and VFS genetic variants do not exhibit altered cardiac contractile function or cardiac hypertrophy following sham surgery treatment. (a) Left ventricular % fractional shortening (LV %FS), (b) left ventricular internal dimension at end-diastole (LVIDd), and (c) heart weight/body weight (HW/BW) ratios are not significantly different between genotypes following sham surgery. (d-g) Representative M-mode analyses for each genotype do not reveal significant contractile defects following sham surgery, as quantitated in a. (h-o) Trichrome staining of hearts from each mouse genotype is not grossly different after sham surgery. (d, h, l) - *WT*; (e, i, m) - *Vcl^{VFS/+}*; (f, j, n) *Tpm1^{TEK/+}*; (g, k, o) *TV-Dhet*. Data presented as interquartile range (box), surrounding data mean at center line with whiskers representing minimum and maximum of data set, with superimposed individual data points. One-sided ANOVA with Tukey multiple correction test alpha $p > 0.05$ (n.s.) across all comparisons. Complete quantitative data presented in Supplementary Table 7. 2 mm scale bars. n = 5 animals in *WT* and *Vcl^{VFS/+}* genotypes, n = 6 in *Tpm1^{TEK/+}* and *TV-Dhet* genotypes. Data presented in panels d, e, h, i, l, m were repeated independently 5 times with similar results. Data presented in panels f, g, j, k, n, o were repeated independently 6 times with similar results.



Supplementary Figure 12. No significant difference is observed in cardiomyocyte size or fibrosis area across different mouse conditions. (a) Wheat germ agglutinin (green) staining of cardiac sections from 58 week old mice as well as Post-Sham or Post-TAC mice, reveals no significant difference in cardiomyocyte cross-sectional area across all studied genotypes and cardiac conditions (i.e. 58 weeks, Post-Sham and Post-TAC), as quantitated in **b**. Nuclei were stained with DAPI (blue). (n = 3 mice and 100 cardiomyocytes per genotype, for each condition). (c) Quantitation of cardiac fibrosis area from Figure 4i, j and Supplementary Figure 11h-o showed no significant difference in fibrosis across all studied genotypes and cardiac conditions (i.e. 58 weeks, Post-Sham and Post-TAC). One-sided ANOVA with Tukey multiple correction statistic was used to compare genotypes; no comparison yielded test alpha of $p < 0.05$, “n.s.” indicates no statistically significant comparison. (n = 3-4 in 58 week mice, n = 4 in Post-Sham mice, n = 7-10 in Post-TAC mice).

Supplementary Table 1

<i>TPMI</i> Off-Target Loci Analyzed		
Genome Locus	Mismatches	Sequence
ch20:32560012-32560034	3[3:9:10]	GGAGGAGGAGGACAAGAAGGCAG
ch6:83864877-83864899	4[1:3:5:10]	TGAGCAGGCAGACAAGAAGGTAG
ch2:181678740-181678762	4[2:3:4:10]	GCACGAGGCAGACAAGAAGGAGG
ch5:14504528-14504550	3[1:3:17]	CGAGGAGGCCGACAAGCAGGGGG
ch8:12590066-12590088	3[3:10:17]	GGTGGAGGCAGACAAGCAGGTAG
ch8:8076935-8076957	3[3:10:17]	GGTGGAGGCAGACAAGCAGGTAG
ch7:99391076-99391098	3[4:7:20]	GGCTGATGCCGACAAGAAGATGG
ch9:35689724-35689746	3[4:7:20]	GGCCGAAGCCGACAAGAAGCAAG
ch1:44496912-44496934	3[3:9:11]	GGAGGAGGACCACAAGAAGGTGG
ch17:51401637-51401659	4[2:3:7:10]	GTGGGAAGCGGACAAGAAGGAAG
<i>VCL</i> Off-Target Loci Analyzed		
Genome Locus	Mismatches	Sequence
ch1:159181747-159181769	3[3:11:20]	CCTCCTGGTGCTAATGCACCAAG
ch10:65341472-65341494	4[2:3:4:20]	CTCTCTGGTGATAATGCACACAG
ch22:22592207-22592229	4[1:3:10:20]	TCCCCTGGTCATAATGCACCAGG
ch5:173249933-173249955	4[1:5:8:17]	ACACTTGATGATAATGTACGAAG
ch2:45533537-45533559	3[8:12:20]	CCACCTGCTGAAAATGCACCTGG
ch2:219015315-219015337	4[1:8:9:12]	ACACCTGAGGAGAATGCACGCAG
ch2:21053610-21053632	4[2:5:9:12]	CTACTTGGGGAAAATGCACGAAG
ch8:40769566-40769588	4[1:2:4:15]	TGAGCTGGTGATAAAGCACGCAG
ch20:24313287-24313309	4[1:2:11:20]	AAACCTGGTGGTAATGCCTGGG
ch3:127304517-127304539	4[3:9:10:12]	CCTCCTGGGTACAATGCACGTAG

Supplementary Table 1. There is no evidence of off-target CRISPR activity in genome-edited H9 hESC lines at computationally predicted off-target sites. The top ten off-target loci for each gRNA used for hESC genome-editing were computationally predicted as previously described⁶. Genome loci, number of mismatches (with respective positions in guide sequence), and sequence of top ten putative off-target sites for the *TPMI* and *VCL* targeting gRNAs are displayed. No change from reference sequence was detected at these loci or in the surrounding region by Sanger sequencing of genome-edited hESC lines.

Supplementary Table 2 (separate file). Differentially expressed genes revealed by RNA-seq of *TV-Dhet* and control (*CTRL*) hiPSC-cardiomyocytes. Genes are shown that met criteria for differential expression between *CTRL* and *TV-Dhet* hiPSC-cardiomyocyte biological replicates including minimum base mean count (100), < 0.8 or > 1.2 fold expression change, and adjusted p-value < 0.01 . Normalized average count across 6 samples represented as Base Mean value. Fold Change in *TV-Dhet* hiPSC-cardiomyocytes normalized to *CTRL* hiPSC-cardiomyocytes. p-value calculated using Wald test with Benjamini-Hochberg procedure false discovery rate adjustment.

Supplementary Table 3

<i>VCL</i> Exon	Percent Spliced In (%)	
	<i>CTRL</i> hiPSC CMs	<i>TV-Dhet</i> hiPSC CMs
Exon 1	100	100
Exon 2	99.6	100
Exon 3	100	100
Exon 4	100	100
Exon 5	100	100
Exon 6	100	100
Exon 7	100	100
Exon 8	100	100
Exon 9	100	100
Exon 10	100	100
Exon 11	100	100
Exon 12	100	100
Exon 13	100	100
Exon 14	100	100
Exon 15	100	100
Exon 16	100	100
Exon 17	100	100
Exon 18	100	100
Exon 19	9.9	13.7
Exon 20	100	100
Exon 21	100	100
Exon 22	100	100

Supplementary Table 3. Percent spliced in analysis of the *VCL* transcript reveals that the exon harboring the *VCL* c.659dupA (*VFS*) variant is not differentially expressed between *CTRL* and *TV-Dhet* hiPSC cardiomyocytes. Exon inclusion, shown as percent spliced in (%) from RNA-seq analysis of the *VCL* transcript, reveals 100% inclusion of exon 6, which harbors the *VFS* variant in both *CTRL* and *TV-Dhet* hiPSC cardiomyocytes (CMs). Exon 19 is alternatively spliced into the *VCL* transcript to generate Metavinculin, which is expressed as a minor isoform in the myocardium.

Supplementary Table 4

<i>Tpm1</i> Off-Target Loci Analyzed		
Genome Locus	Mismatches	Sequence
ch8:91820681-91820703	2[10:13]	ATAAGAAGGAGGAGGAAGACAGG
ch7:30081247-30081269	4[2:3:10:20]	AACAGAAGGGGGCGGAAGAGAAG
ch6:94835335-94835357	4[2:3:10:17]	AGGAGAAGGAGGCGGAGGACTAG
ch9:101371264-101371286	4[2:3:10:13]	AAGAGAAGGGGGAGGAAGACAAG
ch2:169787861-169787883	4[2:3:10:13]	AGCAGAAGGTGGAGGAAGACAAG
ch7:69905020-69905042	4[3:8:10:13]	ATGAGAAAGGGGAGGAAGACAAG
ch12:99574536-99574558	4[2:8:9:11]	AAAAGAATTCAGCGGAAGACAAG
ch2:62596992-62597014	3[6:11:20]	ATAAGGAGGCTGCGGAAGAAGGG
ch19:57744331-57744353	4[2:3:10:15]	AGTAGAAGGGGGCGAAAGACAAG
ch18:27893369-27893391	4[1:4:6:13]	GTATGGAGGCGGGGGAAGACCAG
<i>Vcl</i> Off-Target Loci Analyzed		
Genome Locus	Mismatches	Sequence
ch3:124227527-124227549	3[4:7:8]	TCACAGTGTCTTCTATTCCCTGGG
ch1:123019822-123019844	3[3:7:10]	TCTAAGATTTTTCTATTCCCTGAG
chX:77664398-77664420	3[1:4:11]	ACAGAGCTTCTTCTATTCCCTAAG
ch7:74071960-74071982	3[5:8:20]	TCAATGCATCTTCTATTCCAAAG
ch9:78860453-78860475	2[11:19]	TCAAAGCTTCATCTATTTCATGAG
ch5:80042070-80042092	3[4:8:12]	TCACAGCATCTGCTATTCCCTAGG
ch18:44421445-44421467	4[3:5:8:10]	TCCAGGCATTTTCTATTCCCTTGG
ch13:101989295-101989317	3[8:10:11]	TCAAAGCCTTCTTCTATTCCCTAGG
ch1:3724732-3724754	4[2:3:4:7]	TTTGAGTTTCTTCTATTCCCTTGG
ch1:50956486-50956508	4[1:4:7:10]	CCACAGATTTTTCTATTCCCTCAG

Supplementary Table 4. There is no evidence of off-target CRISPR editing in F0 mice at computationally predicted off-target sites. The top ten off-target loci for each gRNA used for mouse genome-editing were computationally predicted as previously described⁶. Genome loci, number of mismatches (with respective positions in guide sequence), and loci sequence of top ten putative off-target sites for the *Tpm1* and *Vcl* targeting gRNAs are displayed. No change from reference sequence was detected at these loci or in the surrounding region by Sanger sequencing of genome-edited mice.

Supplementary Table 5

Age	17 Weeks		58 Weeks	
Genotype	<i>WT</i> n = 14	<i>Tpm1^{TEK/TEK}</i> n = 12	<i>WT</i> n = 7	<i>Tpm1^{TEK/TEK}</i> n = 7
BW (g)	31.36±1.09	30.08±1.67	43.57±3.24	45.86±1.20
HR (bpm)	586±15	578±19	612±11	583±17
LVIDd (mm)	3.39±0.10	3.57±0.10	3.52±0.10	3.82±0.14
LVIDs (mm)	2.12±0.12	2.37±0.10	2.05±0.08	2.86±0.16*** p=0.0005
LV %FS	37.91±2.28	34.03±1.70	42.00±1.29	25.46±1.96**** p=1.35e-5
IVSd (mm)	0.78±0.01	0.78±0.02	0.89±0.02	0.75±0.01*** p=0.0002
LVPWd (mm)	0.72±0.01	0.75±0.02	0.82±0.04	0.74±0.02

Supplementary Table 5. Echocardiographic analysis of *WT* and *Tpm1^{TEK/TEK}* mice at 17 and 58 weeks reveals decreased contractility in *Tpm1^{TEK/TEK}* mice. 58 week *Tpm1^{TEK/TEK}* mice exhibit reduced contractility [left ventricular % fractional shortening (LV %FS)] when compared to *WT* mice. Additional abbreviations used: Body weight (BW), Heart rate (HR) in beats per minute (bpm), Left ventricular internal dimension at end-diastole (LVIDd), Left ventricular internal dimension at end-systole (LVIDs), Interventricular septum thickness at end-diastole (IVSd), Left ventricular posterior wall thickness at end diastole (LVPWd). Data presented as mean +/- SEM. Student's two-sided *t*-test alpha **p* < 0.05, ***p* < 0.01, ****p* < 0.001, *****p* < 0.0001 when compared to *WT* measurements of same age (all significant values shaded in gray, all other comparisons were not statistically significant).

Supplementary Table 6

Age	15 Weeks				58 Weeks			
Genotype	<i>WT</i> n = 10	<i>Vcl^{VFS/+}</i> n = 8	<i>Tpm1^{TEK/+}</i> n = 9	<i>TV-Dhet</i> n = 9	<i>WT</i> n = 7	<i>Vcl^{VFS/+}</i> n = 7	<i>Tpm1^{TEK/+}</i> n = 7	<i>TV-Dhet</i> n = 6
BW (g)	15.57±0.84	14.00±0.85	14.74±0.42	14.44±0.45	43.57±3.25	45.86±3.22	45.00±3.85	45.83±3.10
HR (bpm)	591±17	592±15	611±19	585±18	655±46	627±10	572±20	657±26
LVIDd (mm)	3.40±0.13	3.42±0.11	2.99±0.15‡ p=0.0169	3.57±0.11	3.52±0.10	3.03±0.16	3.83±0.19§§ p=0.006	3.72±0.16§ p=0.0279
LVIDs (mm)	2.09±0.18	2.10±0.09	1.84±0.14	2.38±0.12	2.05±0.08	1.82±0.15	2.58±0.19§§ p=0.0084	2.61±0.13§§ p=0.0085
LV %FS	39.40±2.95	38.63±1.30	38.86±2.03	33.60±2.26	42.00±1.29	40.51±2.24‡ p=0.0251	33.26±2.93	29.48±3.20** p=0.0097
IVSd (mm)	0.81±0.02	0.76±0.03	0.79±0.02	0.77±0.01	0.89±0.02	0.89±0.03	0.90±0.03	0.84±0.04
LVPWd (mm)	0.73±0.02	0.67±0.03	0.71±0.01	0.72±0.01	0.82±0.04	0.85±0.02	0.84±0.04	0.82±0.04

Supplementary Table 6. Echocardiographic analysis of mice at 15 and 58 weeks reveals decreased contractility in *TV-Dhet* mice with aging. Only *TV-Dhet* mice exhibit reduced contractility [left ventricular % fractional shortening (LV %FS)] at 58 weeks when compared to *WT* mice. Left ventricular internal dimension at end-diastole (LVIDd) was not significantly different between *WT* mouse hearts and mouse hearts harboring *TEK*, *VFS*, or *TV-Dhet* variants. Additional abbreviations used: Body weight (BW), Heart rate (HR) in beats per minute (bpm), Left ventricular internal dimension at end-systole (LVIDs), Interventricular septum thickness at end-diastole (IVSd), Left ventricular posterior wall thickness at end diastole (LVPWd). Data presented as mean +/- SEM. One-sided ANOVA with Tukey multiple correction test alpha *p < 0.05, **p < 0.01 vs *WT* of same condition. ‡p < 0.05 vs *TV-Dhet* of same condition, §p < 0.05, §§p < 0.01 vs *Vcl^{VFS/+}* of same condition (all significant values shaded in gray, all other comparisons were not statistically significant).

Supplementary Table 7

Genotype	<i>WT</i>			<i>Vcl^{VFS/+}</i>			<i>Tpm1^{TEK/+}</i>			<i>TV-Dhet</i>		
Condition	Pre-Surg n = 21	Post-TAC n = 16	Post-Sham n = 5	Pre-Surg n = 19	Post-TAC n = 14	Post-Sham n = 5	Pre-Surg n = 24	Post-TAC n = 18	Post-Sham n = 6	Pre-Surg n = 21	Post-TAC n = 15	Post-Sham n = 6
BW (g)	27.86±0.92	26.16±0.90	26.60±0.87	27.32±0.75	24.61±0.91	24.60±0.68	26.75±0.44	25.03±0.68	25.17±0.48	28.57±0.51	25.11±0.54	28.00±0.93
HR (bpm)	594±12	607±10	634±17	615±10	572±24	658±14	581±13	560±21	653±15	617±13	572±18	646±15
LVIDd (mm)	3.29±0.07	3.69±0.01	3.32±0.22	3.30±0.10	3.84±0.09‡ p=0.0372	3.20±0.07	3.41±0.06	3.98±0.11	3.26±0.08	3.48±0.06	4.24±0.08** p=0.0014	3.23±0.08
LVIDs (mm)	2.12±0.07	2.72±0.16	1.93±0.20	2.03±0.09	3.01±0.14‡ p=0.0221	1.87±0.08	2.20±0.06	3.09±0.09‡ p=0.0428	1.94±0.06	2.20±0.05	3.56±0.12*** p=0.0001	2.03±0.10
LV %FS	35.71±1.21	26.94±2.55	42.4±2.77	38.98±1.60	21.95±1.97	41.38±2.46	35.49±1.24	22.36±1.19	40.55±1.20	36.83±1.10	16.19±1.52*** p=0.0008	37.23±2.36
IVSd (mm)	0.76±0.01	1.05±0.02	0.76±0.02	0.77±0.01	1.00±0.03	0.77±0.03	0.78±0.02	1.01±0.03	0.75±0.02	0.76±0.01	0.97±0.03	0.81±0.04
LVPWd (mm)	0.70±0.01	1.03±0.03	0.71±0.02	0.70±0.01	0.98±0.03	0.70±0.02	0.72±0.01	1.05±0.03	0.71±0.01	0.70±0.01	0.97±0.04	0.74±0.03

Supplementary Table 7. Echocardiographic analysis of Pre-Surgery (Pre-Surg), Post-TAC and Post-Sham mice reveals an exaggerated myocardial response in *TV-Dhet* mice compared to controls following TAC surgery. Contractile function, as assayed by left ventricular % fractional shortening (LV %FS), is significantly reduced in Post-TAC *TV-Dhet* mice compared to Post-TAC *WT* mice. Although not statistically significant, there is a consistent trend that Post-TAC *Tpm1^{TEK/+}* and *Vcl^{VFS/+}* contractility is reduced compared to that of Post-TAC *WT* mice but is greater than that of Post-TAC *TV-Dhet* mice. Additionally, left ventricular internal dimension at end-diastole (LVIDd) is significantly increased in *TV-Dhet* mouse hearts following TAC, compared to *WT* and *Vcl^{VFS/+}*. Following TAC surgery, an expected decrease in contractility, increase in measures of left ventricular chamber dimensions, and increase in wall thickness, was observed across all genotypes compared to Pre-Surg (Pre-TAC and Pre-Sham) conditions confirming haemodynamic stress induced by TAC surgery. Additional abbreviations used: Body weight (BW), Heart rate (HR), beats per minute (bpm), Left ventricular internal dimension at end-systole (LVIDs), Interventricular septum thickness at end-diastole (IVSd), Left ventricular posterior wall thickness at end diastole (LVPWd). Data presented as mean +/- SEM. One-sided ANOVA with Tukey multiple correction test alpha *p < 0.05, **p < 0.01, ***p < 0.001, vs *WT* of same condition. ‡p < 0.05, ‡‡p < 0.01 vs *TV-Dhet* of same condition. There was no significant difference between Pre-Surg and Post-Sham mice of the same genotype across all parameters (all significant values shaded in gray, all other comparisons were not statistically significant).

Supplementary Table 8. (separate file) Primers, guideRNA (gRNA), and single strand DNA oligonucleotide (ssDNA) sequences.

Supplementary Movies

Supplementary Movie 1. Representative parasternal short axis left ventricular views of mouse echocardiography Pre-Surg for *WT* mice. This experiment was independently repeated 21 times with similar results.

Supplementary Movie 2. Representative parasternal short axis left ventricular views of mouse echocardiography Post-TAC for *WT* mice. This experiment was independently repeated 16 times with similar results.

Supplementary Movie 3. Representative parasternal short axis left ventricular views of mouse echocardiography Pre-Surg for *Vcl*^{VFS/+} mice. This experiment was independently repeated 19 times with similar results.

Supplementary Movie 4. Representative parasternal short axis left ventricular views of mouse echocardiography Post-TAC for *Vcl*^{VFS/+} mice. This experiment was independently repeated 14 times with similar results.

Supplementary Movie 5. Representative parasternal short axis left ventricular views of mouse echocardiography Pre-Surg for *Tpm1*^{TEK/+} mice. This experiment was independently repeated 24 times with similar results.

Supplementary Movie 6. Representative parasternal short axis left ventricular views of mouse echocardiography Post-TAC for *Tpm1*^{TEK/+} mice. This experiment was independently repeated 18 times with similar results.

Supplementary Movie 7. Representative parasternal short axis left ventricular views of mouse echocardiography Pre-Surg for *TV-Dhet* mice. This experiment was independently repeated 21 times with similar results.

Supplementary Movie 8. Representative parasternal short axis views of *TV-Dhet* mouse echocardiography reveals grossly decreased left ventricular function Post-TAC. This experiment was independently repeated 15 times with similar results.

Supplementary References

- 1 Schrodinger, LLC. *The PyMOL Molecular Graphics System, Version 1.8* (2015).
- 2 Olson, T. M., Kishimoto, N. Y., Whitby, F. G. & Michels, V. V. Mutations that alter the surface charge of alpha-tropomyosin are associated with dilated cardiomyopathy. *Journal of molecular and cellular cardiology* **33**, 723-732, doi:10.1006/jmcc.2000.1339 (2001).
- 3 Kong, A. & Cox, N. J. Allele-sharing models: LOD scores and accurate linkage tests. *Am J Hum Genet* **61**, 1179-1188, doi:10.1086/301592 (1997).
- 4 Purcell, S., Cherny, S. S. & Sham, P. C. Genetic Power Calculator: design of linkage and association genetic mapping studies of complex traits. *Bioinformatics* **19**, 149-150 (2003).
- 5 Lian, X. *et al.* Directed cardiomyocyte differentiation from human pluripotent stem cells by modulating Wnt/ β -catenin signaling under fully defined conditions. *Nature protocols* **8**, 162-175, doi:10.1038/nprot.2012.150 (2013).
- 6 Hsu, P. D. *et al.* DNA targeting specificity of RNA-guided Cas9 nucleases. *Nature biotechnology* **31**, 827-832, doi:10.1038/nbt.2647 (2013).